Recent land cover changes in the Southwestern US lead to an increase in surface temperature

Tomer Duman [*], Cheng-Wei Huang, Marcy E. Litvak

Department of Biology, University of New Mexico, Albuquerque, NM, 87131, USA

ARTICLE INFO

ABSTRACT

The increase in large-scale land cover change (LCC) in recent decades, particularly in response to climate-driven disturbances, has potential to impact local and regional changes in climate due to modification of carbon sources and sinks, albedo, surface roughness and energy fluxes. Using observational data, we predict the impact of two of the most extensive LCCs occurring in the Southwestern US: drought-induced tree mortality and shrub encroachment into grasslands, on surface temperature. We developed a new energy balance method that extracts the biophysical responses to environmental conditions, to predict how structural changes in albedo, surface roughness and canopy conductance following LCC will alter surface temperature. This method allows us not only to explain the observed differences in surface temperature between two non-adjacent study sites with different environmental conditions, but also to separate the contribution of biophysical and non-biophysical properties to surface temperature. Our results suggest that changes in biophysical properties due to shrub encroachment and tree mortality in the Southwestern US (independent of changes in other environmental properties) can potentially lead to an increase in midday surface temperature (11AM to 2PM) of 1 to 2 degrees Celsius, comparable to changes in surface temperature following deforestation. Although the average surface temperature increase in response to both shrub encroachment and tree mortality is similar, the biophysical properties driving the temperature change are different in each scenario. Change in aerodynamic conductance following tree mortality is the largest contributor to heating, while reduced albedo and canopy conductance drive the increase in surface temperature following shrub encroachment. We also show how this increase in daytime surface temperature could be further intensified with future climate, especially with the expected reduction in soil water availability in the Southwest.

1. Introduction

Extensive land cover changes (LCC) are one of the main drivers leading to climate change, as they modify terrestrial carbon sinks and sources, and therefore global atmospheric gas composition (Li et al., 2013; Zhao and Jackson, 2014; Devaraju et al., 2015; Winckler et al., 2016). However, LCC can also influence local and regional climate through changes in biophysical characteristics such albedo, surface roughness, and ecosystem transpiration rate (Bonan, 2008; Pielke et al., 2011), that directly impact surface temperature (Juang et al., 2007; Lee et al., 2011; Baldocchi and Ma, 2013; Luyssaert et al., 2014; Zhang et al., 2014; Zhao and Jackson, 2014; Vanden Broucke et al., 2015). The relationship between land cover change and surface temperature has been most extensively studied in response to both deforestation and afforestation, due to the relevance of these LCCs for climate mitigation

(Bonan, 2008; Bathiany et al., 2010; Davin and de Noblet-Ducoudré, 2010; Li et al., 2013; Mahmood et al., 2014; Devaraju et al., 2015). However, an increase in other large-scale LCCs in recent decades, particularly those driven by changes in climate and/or management (Matthews et al., 2004; Levis, 2010; Baldocchi and Ma, 2013; Williams et al., 2013; Anderegg et al., 2015) highlights the need to examine the potential impact the changes in biophysical properties driven by these LCCs may also have on land surface temperature.

The Southwestern US, in particular, has been experiencing large-scale shifts in land cover in recent decades, many of them driven by a combination of extreme droughts starting at the turn of the century with anomalously high air temperatures (Seager et al. 2007; Williams et al. 2013). Fire and insect outbreaks combined have caused high levels of mortality and driving large structural changes in more than 14% of Southwest forest areas since the beginning of the century (Williams

---

et al., 2010; Shaw et al., 2005; Breshears et al., 2009; Van Mantgem et al., 2009; Clifford et al., 2011; Swetnam and Betancourt, 1998; Raffa et al., 2008; Romme et al., 2009; Westerling and Swetnam, 2003; Westerling et al., 2006;). In other areas in the Southwest, shrubs and other woody species have been invading semi-arid grasslands at an unparalleled rate over the past few decades driven by changes in elevated CO_2, grazing and fire suppression (Buffington and Herbel, 1965; Van Auken, 2009; D'Odorico et al., 2010; He et al., 2010; Petrie et al., 2015; Biederman et al., 2017). More than 50 million ha that were previously semiarid Southwestern grasslands are now covered by woody shrubs (Van Auken, 2000). Both of these shifts in land cover, from grassland to shrubland, and from intact forest to a disturbed one following tree mortality, are associated with large changes in structure, and therefore, the biophysical properties of these biomes. The large extent of these land cover changes in the Southwestern US in recent decades, and the predicted increase in drought and air temperature in the coming decades (Seager et al. 2007; Cayan et al., 2010; Williams et al. 2013; Cook et al., 2015), increases the importance of quantifying the potential impact of these LCCs on surface temperature, and understanding the underlying processes that are driving this change.

Surface energy balance methods are often used to explore the potential effects of LCC on surface temperature and quantify the contribution of perturbations in the biophysical characteristics to these temperature changes (Juang et al., 2007; Lee et al., 2011; Rigden and Li, 2017). This is commonly done by measuring all components required for calculating energy balance at two nearby sites with similar external forcings, such as air temperature, incoming radiation, and precipitation (Chen and Dirmeyer, 2016). Previous studies typically use two nearby sites for this comparison - an undisturbed site and a manipulated/cleared site (Luyssaert et al., 2014; Vanden Broucke et al., 2015; Chen and Dirmeyer, 2016; Burakowski et al., 2018; Devaraju et al., 2018; Liao et al., 2018), therefore satisfying conservation of environmental factors. However, no two sites have the exact same environmental conditions. Several studies have addressed this discrepancy by including the site to site differences in non-biophysical variables, such as air temperature and ground heat flux (Chen and Dirmeyer, 2016; Liao et al., 2018), but this approach does not allow us to predict changes in surface temperature under anything other than the observed conditions. The ability to quantify the contribution of LCC induced structural change, independent of environmental factors, is important to predict changes in surface temperature in response to both LCC and future climate change.

Here we developed a new methodology to predict changes in surface temperature following LCC that are driven only by perturbations in biophysical characteristics. The novelty of this method is that it allows us to use two sites that are not necessarily adjacent or experience similar environmental conditions. We used data mining from existing eddy covariance sites with continuous, long-term land-atmosphere energy flux data that structurally represent end members of LCC scenarios. In each site, we extracted the biophysical responses of albedo, canopy conductance and aerodynamic conductance to measured environmental conditions. We then used these data to simulate pre-LCC and post-LCC time series to evaluate the change in surface temperature when biophysical properties are altered, but environmental factors are conserved.

With this new approach, we predict the potential surface temperature change driven by two specific types of extensive LCCs common in the Southwestern US in recent decades: 1) piñon mortality in piñon-juniper (PJ) woodlands, and 2) creosote encroachment into desert grasslands. PJ woodlands cover 40 million hectares across the western US (Romme et al., 2009). Mortality of piñon pine in PJ woodlands has recently increased in the Southwestern US, driven by a combination of extreme droughts starting at the turn of the century with anomalously high air temperatures and increased outbreaks of *Piñon ips* bark beetle. Recent studies have highlighted the impact of piñon mortality on both the structure (e.g. stand density, height, species composition, leaf area, bare ground) (Shaw et al., 2005; Breshears et al., 2009; Clifford et al.,

2011; Brewer et al., 2017) and function (gross primary productivity, sensitivity to drought, partitioning of ET) of PJ woodlands (Warnock et al., 2016; Morillas et al., 2017; Krofcheck et al. 2014; Huang et al. 2020). Creosote (*Larrea tridentata*) is one of the most dominant native shrub species in the Southwestern US, and has been expanding at the northern boundary of the Chihuahuan Desert, encroaching into previously C4-dominated grassland, driving changes in dominant plant functional type, vegetation structural parameters (e.g. height, leaf area, leaf color), and bare ground (Báez and Collins, 2008; D'Odorico et al., 2010; He et al., 2010, 2015; Caracciolo et al. 2016). More than 19 million hectares of grassland have been invaded by creosote in the last century (Van Auken, 2000).

We divided the impacts of piñon mortality on surface temperature into two scenarios, the short-term outcome where dead piñon snags are still standing, and the potential long-term scenario assuming complete transition from piñon-juniper woodland to juniper savanna (no regeneration of piñon), with no woody understory. Assuming conservation of environmental forcings, and changes only in biophysical properties, we hypothesized the largest impact on surface temperature following piñon mortality in the short term will be reduced evapotranspiration, which should lead to a small increase in daytime surface temperature. We assumed that albedo and aerodynamic resistance would not be sufficiently different enough in the short-term to modify surface temperature. In the long term, we predicted that complete transition to juniper savanna, assuming no significant change in understory, will result in a larger increase in daytime land surface temperature, on par with what has been observed following deforestation in warm temperate areas (Bonan, 2008; Bathiany et al., 2010; Davin and de Noblet-Ducoudré, 2010; Li et al., 2013; Mahmood et al., 2014; Devaraju et al., 2015). Although albedo would likely increase in this scenario, we predicted this should be counteracted by reduced transpiration and aerodynamic resistance. For our second LCC scenario, shrub encroachment, although we know daytime surface temperature does not differ between existing grass and creosote sites (He et al. 2010), we do not know the specific roles that structural differences vs environmental conditions play in explaining this result from observational data alone. Our method will allow us to predict the change in surface temperature expected with shrub encroachment due only to changes in biophysical properties. We expect that darker colored shrubs replacing lighter colored grasses will decrease albedo and heat the surface. However, we also expected the increase in evapotranspiration often associated with shrub encroachment (Scott et al., 2006; Wang et al., 2018b), to cool and counterbalance the heating from decreased albedo. For both LCC's, we also imposed additional changes in non-biophysical properties, including soil water content, ground heat flux and air temperature to further investigate the roles these parameters may play in explaining differences between observed and predicted changes in surface temperature. This highlights the ability of our new approach to explore the sensitivity of the different ecosystems to additional changes in non-biophysical characteristics following LCC.

2. Study sites and experimental design

We mined data from in five flux tower sites in the New Mexico Elevation Gradient network to construct the end points in our LCC scenarios to quantify the predicted changes in daytime surface temperature due to changes in biophysical characteristics associated with piñon mortality and creosote encroachment. Four of these sites have been AmeriFlux cores sites since 2013 and have been continuously measuring carbon, water and energy fluxes since 2007. These include US-Seg: desert grassland, US-Ses: creosote shrubland, US-Wjs: juniper savanna and US-Mpj: piñon-juniper woodland. The additional site we used is a piñon-juniper woodland (US-Mpg), where all of the piñon were girdled in 2009 as part of a manipulation experiment to quantify the consequences of piñon mortality on PJ-woodland carbon, water and energy fluxes (Krofcheck et al., 2014; Morillas et al., 2017; Huang et al. 2020).

Site images are shown in Fig. 1.

The grass (US-Seg) and creosote shrub (US-Ses) sites are located within the Sevilleta National Wildlife Refuge in central New Mexico. The Sevilleta covers an extensive ≈ 130 km^2, nearly flat, desert area bounded on the east by the Los Piños Mountains and on the west by the Rio Grande river. The grass site is nearly monospecific, dominated by C$_4$ black grama (*Bouteloua eripoda*), that cover about 60% of the surface (D'Odorico et al., 2010; Anderson-Teixeira et al. 2011; Petrie et al. 2014). The shrub site is located about 5 km away from the grassland site, and is dominated by C$_3$ creosote (*Larrea tridentata*) (D'Odorico et al.; 2010 Anderson-Teixera et al. 2013; Petrie et al. 2014). The PJ (US-Mpj) and juniper savanna (US-Wjs) sites are located 45 and 80 km to the east of the Sevilleta National Wildlife Refuge, respectively. The PJ site is dominated by two co-dominant coniferous tree species, *Pinus edulis* and *Juniperus monosperma*. The juniper savanna site consists of open *J. monosperma* tree canopy with an understory of black grama. We also used a PJ site (US-Mpg), separated approximately by 2.4 km from US-Mpj, where piñon girdling manipulation was implemented. The girdling was applied in September 2009 to all large piñon trees (≈ 1630 trees > 7 cm diameter at breast height), resulting in complete needle loss in less than 1 year, reducing total leaf area of piñon per unit ground area from 0.41 to 0.14 m^2 m^{-2} (i.e., 67% reduction). The dead piñon boles stayed standing through the entire measurement period. Additional site characteristics are provided in Table 1.

We used the US-Mpj site to represent the Pre-LCC system for piñon-mortality, before any mortality has occurred. We used the piñon girdled site (US-Mpg), to represent the expected change in ecosystem structure in the decade following piñon mortality. As discussed above, the piñon trees in US-Mpg were girdled in 2009, and at least 80% of the piñon snags are still standing in 2020. We used the US-Wjs site to represent the structural changes we would expect from complete transition from piñon-juniper woodland to juniper savanna, with no significant piñon regeneration or change in understory. We mined data from the grass (US-Seg) and shrub (US-Ses) to reconstruct the biophysical response to shrub encroachment into grasslands.

Meteorological and continuous land-surface carbon, water and energy flux measurements were collected in the grass, shrub, PJ and juniper savanna sites for 11 years, from January 2007 to end of December 2017 and are available as part of the AmeriFlux network (http://ameriflux.lbl.gov, site codes US-Seg, US-Ses, US-Mpj and US-Wjs

respectively). These data were recorded at a frequency of 10 Hz, and stored as 30-minute averages of 4 component radiation (CNR1 or CNR4, Kipp and Zonen, Delft, Netherlands), air temperature and relative humidity (HMP45C, Vaisala, Helsinki, Finland). Latent and sensible heat fluxes were derived from eddy covariance measurements at 10 Hz, using a 3-axis sonic anemometer (CSAT3, Campbell Scientific, Logan, UT, USA) and an open path infrared gas analyzer (Li-7500, LiCor Biosciences; Lincoln, NE, USA). Post-processing of the tower high-frequency data included filtering, despiking, and coordinate rotation. Half hourly fluxes were calculated and the Webb-Pearman-Leuning correction for open-path instruments (Webb et al., 1980) was applied. The wind velocity measurements were used to calculate wind speed and friction velocity. Additionally, ECHO probes (TE 5cm, Decagon Devices, Pullman, WA, 27 per site) were used for the measurements of soil volumetric water content (SWC). In this work, we chose to focus on midday surface temperature, therefore the data were filtered to include times from 11AM to 2PM.

3. New energy balance approach to estimate changes in surface temperature following LCC

3.1. Previous approaches

Earlier studies use the surface energy budget equation to express the surface temperature, T_s (Juang et al., 2007; Lee et al., 2011). They then attribute the change in T_s due to LCC (ΔT_s) to changes in biophysical properties (χ), using a Taylor series expansion:

$$\Delta T_s = \sum_i \frac{\partial T_s}{\partial \chi_i} \Delta \chi_i \qquad (1)$$

The choice of which biophysical properties are used in Eq. 1 depends mostly on the choice of parameterization for the latent and sensible heat fluxes (*LE* and *H* respectively) in the energy budget equation. The two most popular approaches (Juang et al., 2007; Lee et al., 2011) consider changes in albedo $\left(\frac{\partial T_s}{\partial \alpha} \Delta \alpha\right)$, but parameterize *H* and *LE* differently. Lee et al. (2011) consider changes in the aerodynamic resistance $\left(\frac{\partial T_s}{\partial r_a} \Delta r_a\right)$ and in the Bowen ratio $\left(\frac{\partial T_s}{\partial \beta} \Delta \beta\right)$, with β defined as the ratio of sensible to
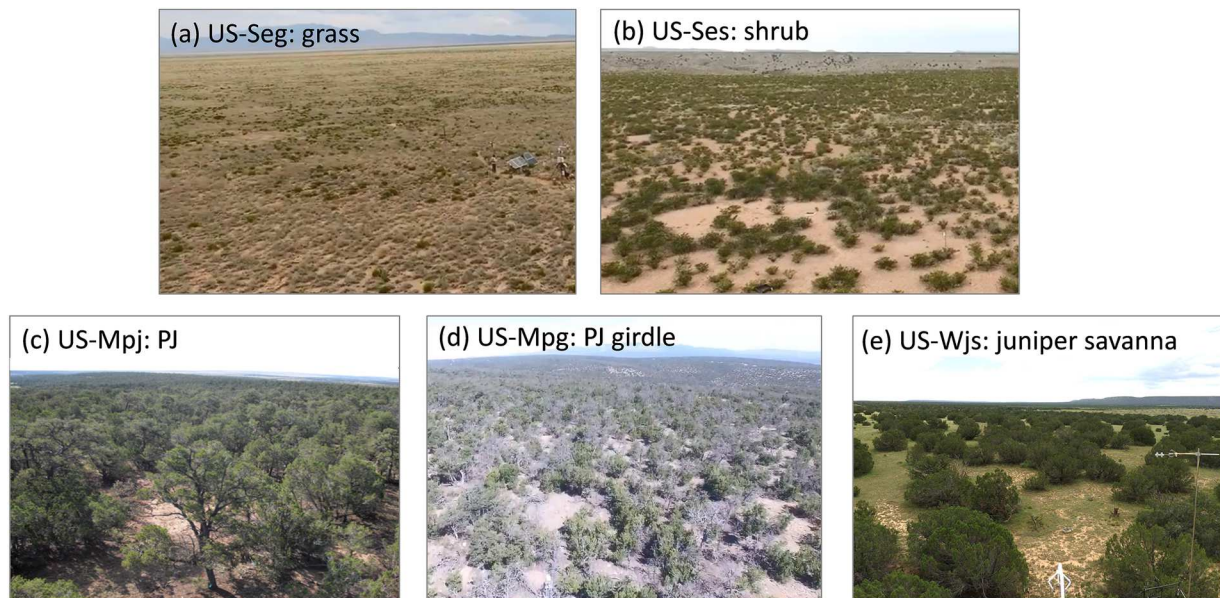

Fig. 1. Images of the study sites – (a) US-Seg: desert grassland, (b) US-Ses: creosote shrubland, (c) US-Mpj: piñon-juniper woodland, (d) US-Mpg: girdle-manipulated piñon-juniper woodland, and (e) US-Wjs: juniper savanna.

Table 1
Site elevation, height of the eddy covariance system (sensor height), average height of the canopy, atmospheric pressure at sensor height, mean annual precipitation during the experiment, latitude and longitude for each of the five study sites.

			grass (US-Seg)	shrub (US-Ses)	PJ (US-Mpj)	PJ girdle (US-Mpg)	juniper savanna (US-Wjs)
site elevation	A	[m]	1596	1604	2196	2160	1931
sensor height	z	[m]	3.2	3.2	8.2	7.6	10.4
canopy height	h	[m]	0.25	0.8	4.0	4.0	3.0
air pressure	p_a	[kPa]	83.4	83.3	77.5	77.5	80.0
mean annual temperature	MAT	[°C]	17.7	17.7	14.8	14.8	15.2
latitude			34.3623	34.3349	34.4385	34.4468	34.4254
longitude			-106.7020	-106.7442	-106.2377	-106.2135	-105.8615

latent heat fluxes. Juang et al. (2007), on the other hand, lump the two effects into one parameter (η), which they call the bulk aerodynamic conductance.

When comparing two nearby sites, the contribution of changes in biophysical properties can be calculated directly from measurements. α at each site can be calculated from shortwave radiation, and r_a, β or η from H and LE. Even when there are other differences at two study sites, such as in air temperature (ΔT_a) or in ground heat flux (ΔG_s), their contribution to ΔT_s can be quantified by including additional terms $\left(\frac{\partial T_s}{\partial T_a} \Delta T_a \text{ and } \frac{\partial T_s}{\partial G_s} \Delta G_s \right)$ in Eq. 1 (Liao et al., 2018). However, in that case, this approach cannot predict ΔT_s if there are only changes in the biophysical properties, since changes in non-biophysical properties (e.g. ΔT_a or ΔG_s) will disturb the energy balance of the system, thereby affecting the surface temperature.

3.2. New approach for estimating ΔT_s

We suggest a new approach to isolate the impact of changes in biophysical properties on surface temperature, when the two study sites also differ in non-biophysical properties. In this approach we reconstruct the response of the biophysical properties to environmental controls from the measured data. Therefore, rather than assuming that H and LE are related through β or η, which both have a complicated and unpredictable response to soil water content (SWC) or vapor pressure deficit (D), we parameterize H and LE separately. We chose the following parameterization:

$$H = g_a c_p (T_s - T_a) \tag{2}$$

$$LE = g_T L_V D / p_a \tag{3}$$

where $g_a = 1/r_a$ and $g_T = 1/(r_a + r_c)$. g_a and g_T are the aerodynamic and total canopy conductance, and r_a and r_c are the aerodynamic and canopy resistances. This approach is similar to the one used in Rigden and Li (2017). Since $r_c >> r_a$ during midday, we chose to simplify the parameterization of LE, using $g_T \approx g_c$, where $g_c = 1/r_c$ is the canopy conductance. c_p is the specific heat of air, L_V is the latent heat of vaporization, and p_a is the atmospheric pressure at the measurement height (Table 1). According to our parametrization, the biophysical properties we consider in this work are g_c, g_a and α.

To estimate the change in T_s, we first capture the biological response of the canopy conductance to both vapor pressure deficit and soil water content. The response of g_c was determined for each site, by fitting the half-hourly data to $g_c = g_{ref} - m\log D$ (m is the slope between g_c and $\log D$, and g_{ref} is g_c at $D=1$kPa), after binning the data into four equally sized SWC categories (0 to 25, 25 to 50, 50 to 75, and 75 to 100 percentiles of the data). Figure S1 in Supplementary Material shows the data and the fitted lines for g_c at the sites studied here). Next, the response of g_a is linked to the horizontal wind speed (U) and the momentum and heat roughness lengths (z_m and z_h). The roughness lengths are related to phenology, and thereby determined on a monthly basis. We evaluated 12 monthly values for z_m by regressing $U = u_* k^{-1} \log((z-d)/z_m)$ to match the mean horizontal wind speed U, using all the half-hourly data

from each specific month from the original sites, during our time record. u_* is the friction velocity, k is the von-Karman constant, z is the sensor height (Table 1), and d is the vegetation displacement height ($d = 0.7h$, h is the canopy height specified in Table 1). Similarly, 12 monthly values for z_h were obtained by regressing $T_s - T_a = H(k\rho c_p u_*)^{-1} \log((z-d)/z_h)$ to match the mean surface temperature T_s (ρ is the air density). These roughness lengths describe a representative year and are presented in Fig. S1. We also calculated albedo on a monthly scale from each site's incoming and outgoing shortwave radiation (S_{in} and S_{out}) measurements (Fig. 2).

With the response of g_c to D and SWC, and the monthly scale z_m, z_h and α, we generate half-hourly time-series data for two new simulated sites, referred to as Site$_{pre}$ and Site$_{post}$, indicating pre-conversion and post-conversion respectively. The half-hourly midday data for T_a, S_{in}, L_{in}, D, U_{100} and SWC from the original site, that represents pre-conversion vegetation cover, were used for both Site$_{pre}$ and Site$_{post}$. U_{100} is the mean wind speed at a height of 100 meters, calculated using the logarithmic profile high above the canopy. We assumed U_{100} did not change after conversion, as opposed to U at the sensor height or u_*. Then, the time series of g_c is calculated on a half-hourly basis, from the logarithmic fits ($g_c = g_{ref} - m\log D$) of both original sites, using the identical D and SWC of Site$_{pre}$ and Site$_{post}$. Next, g_a is calculated for both sites on a half-hourly basis by re-evaluating u_* from $U_{100} = u_* k^{-1} \log((100-d)/z_m)$ and then $g_a = k\rho u_*/\log((z-d)/z_h)$, using U_{100} from Site$_{pre}$ and Site$_{post}$ (identical), and monthly z_m and z_h calculated from both original sites. Note that the value of the displacement height d is also updated to represent change in canopy height after conversion.

Finally, to ensure an energy balance at the simulated sites is conserved, G_s for Site$_{pre}$ is calculated according to the surface energy budget equation, using the observed T_s (from L_{out}) with the above parameterization of H and LE Eqs. 2 and (3):

$$S_{in} + L_{in} - \underbrace{\alpha S_{in}}_{S_{out}} - \underbrace{\varepsilon_s \sigma T_s^4}_{L_{out}} = \underbrace{g_a c_p (T_s - T_a)}_{H} + \underbrace{g_c L_V D / p_a}_{LE} + G_s \tag{4}$$

This G_s is then carried on to Site$_{post}$, assuming conservation of ground heat flux.

Finally, Eq. 4 is used again to back-calculate T_s for Site$_{post}$. The estimated ΔT_s due to LCC is the difference between T_s at the simulated Site$_{pre}$ and Site$_{post}$, and is different from the observed ΔT_s at the two original study sites.

Note, that here G_s and SWC are considered as non-biophysical properties and are treated as environmental drivers. In practice, LCC's have a complex inter-related feedback between the fraction of radiation that arrives to the surface, and ground heat capacity and water content. Here, we explore the impact of additional changes in ground heat flux, soil water content, as well as air temperature on changes in surface temperature following LCC, by imposing an incremental increase of 5, 10 and 20 percent in G_s or SWC, or increasing air temperature by 1, 2 and 3°C in Site$_{post}$ compared to Site$_{pre}$. Such sensitivity analysis allows us to explore potential changes in theses co-dependent variables without extensively increasing the model complexity. We further discuss our modeling approach limitations and suggestions for future improvements
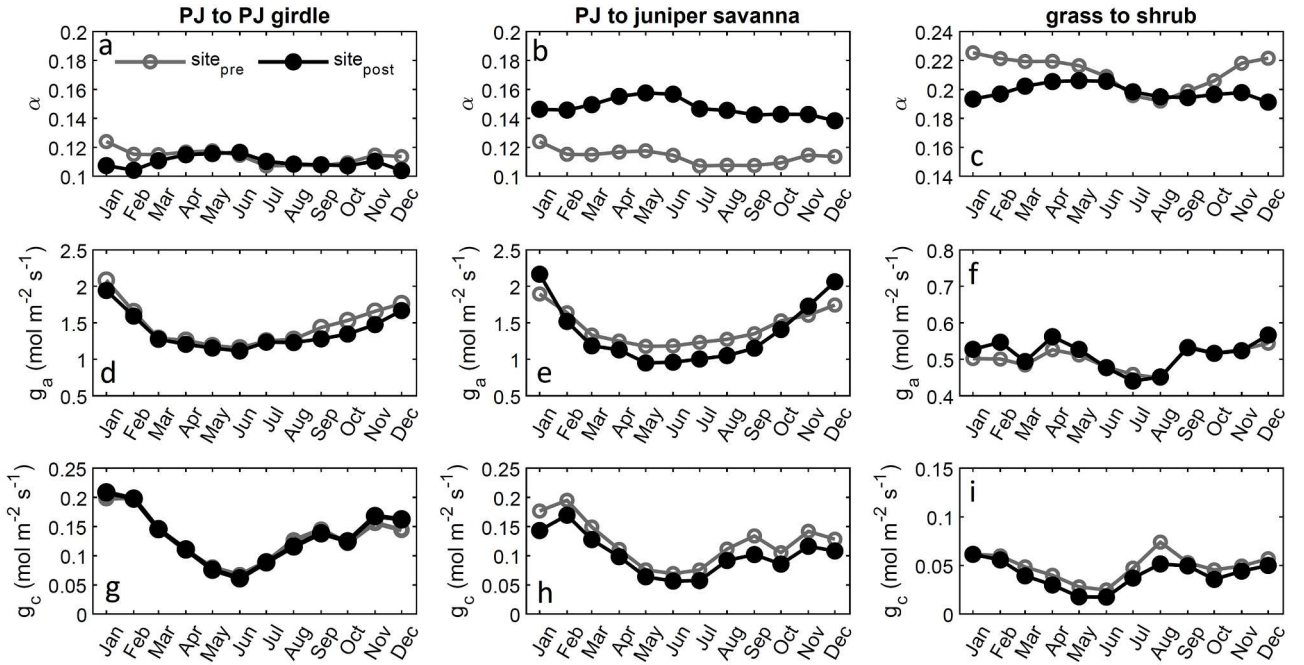
Fig. 2. Monthly average values of the biophysical properties that are affected by LCC: (a,b,c) albedo, (d,e,f) aerodynamic conductance, and (g,h,i) canopy conductance. The data shows a representative year based on 10 years of half hourly values for the simulated Site$_{pre}$ and Site$_{post}$ for the three LCC cases studied: (a,d,g) PJ to PJ girdle, (b,e,h) PJ to juniper savanna, and (c,f,i) grass to shrub.

in Sect. 5.4.

3.3. Attributing ΔT_s to perturbations in biophysical properties

After estimating ΔT_s, we attribute this change in surface temperature to the changes in α, g_a and g_c, following the same approach as in previous energy balance methods. We first linearize the energy balance equation (Eq. 4), using $L_{out} = \varepsilon_s \sigma T_a^4 + 4\varepsilon_s \sigma T_a^3 (T_s - T_a)$, with ε_s representing surface emissivity, and σ the Stefan Boltzmann constant. We use a constant value for ε_s ($= 0.97$), due to the minor role of changes in emissivity on surface temperature (Lee et al., 2011; Rigden et al., 2017). We then reorganize Eq. 4, to express $T_s - T_a$ as:

$$T_s - T_a = \frac{\lambda_0}{1+f}\left(R_n^* - LE - G_s\right)$$

$$R_n^* = S_{in}(1-\alpha) + L_{in} - \varepsilon_s \sigma T_a^4$$

$$LE = g_c L_V \frac{D}{p_a} \tag{5}$$

$$f = \lambda_0 g_a c_p$$

$$\lambda_0 = \frac{1}{4\varepsilon_s \sigma T_a^3}$$

Finally, we use a Taylor series expansion to find the contributions of the perturbation in the biophysical properties to ΔT_s:

$$\Delta T_s = \frac{\partial T_s}{\partial \alpha}\Delta\alpha + \frac{\partial T_s}{\partial g_a}\Delta g_a + \frac{\partial T_s}{\partial g_c}\Delta g_c + \text{(first order terms)}$$

$$\frac{\partial^2 T_s}{\partial\alpha\partial g_a}\Delta\alpha\Delta g_a + \frac{\partial^2 T_s}{\partial g_a\partial g_c}\Delta g_a\Delta g_c + \text{(interaction terms)} \tag{6}$$

$$\frac{1}{2}\frac{\partial^2 T_s}{\partial g_a^2}(\Delta g_a)^2 + \frac{1}{3!}\frac{\partial^3 T_s}{\partial g_a^3}(\Delta g_a)^3 + \dots\text{(higher order terms of } \Delta g_a)$$

Equation 6 is similar to Eq. 1 above, but includes not only the first-order terms in the expansion. Rigden and Li (2017) have shown that assuming independency between the biophysical properties might lead

to errors. Here, we include in the expansion of ΔT_s also interaction terms, as well as higher-order contributions, rather than using only first-order contributions. Note that, according to the formulation of Eq. 5, the third interaction term ($\Delta\alpha\Delta g_c$) and the higher-order terms of Δg_c are zero, and are therefore not included in Eq. 6. For additional information and a full decomposition of ΔT_s see the Supplementary material.

4. Results

We first present the predicted impact of changes in biophysical properties following LCC on surface temperature, and discuss the individual contributions of perturbations in g_a, g_c and α to ΔT_s to this temperature change. Since we also have the surface temperatures measured at our study sites (from long-wave outgoing radiation), we compare the observed ΔT_s with the predicted one, and explain the difference between the two by exploring the sensitivity of the predicted ΔT_s to changes in non-biophysical environmental factors.

4.1. Predicted impact of piñon mortality on T_s

In the short term, our results suggest piñon mortality only slightly impacts all three investigated biophysical variables (albedo, g_a and g_c, see Fig. 2a,d,g). Both before and in the decade after piñon mortality, albedo is relatively constant throughout the year, with a value of 0.114 $\pm$ 0.005. Only a small decrease in albedo (≈ 0.02 decrease) occurred in our model in the coldest winter months (December, January and February). Our results also suggest piñon mortality in the decade following mortality, does not impact calculated g_c (from response curves, Fig. S1). Aerodynamic conductance g_a decreased slightly, starting in September until February. With these mortality-induced perturbations only in the biophysical variables, piñon mortality is predicted to increase daytime surface temperature by $0.55 \pm 0.3°C$ throughout the entire year (Fig. 3a), with Δg_a identified as the main contributor to this increase in the decade following mortality.

In the long term, our results suggest if tree cover at PJ is reduced to density levels observed in the juniper savanna site, albedo would increase by 30% on average, with values of 0.114 ± 0.005 and
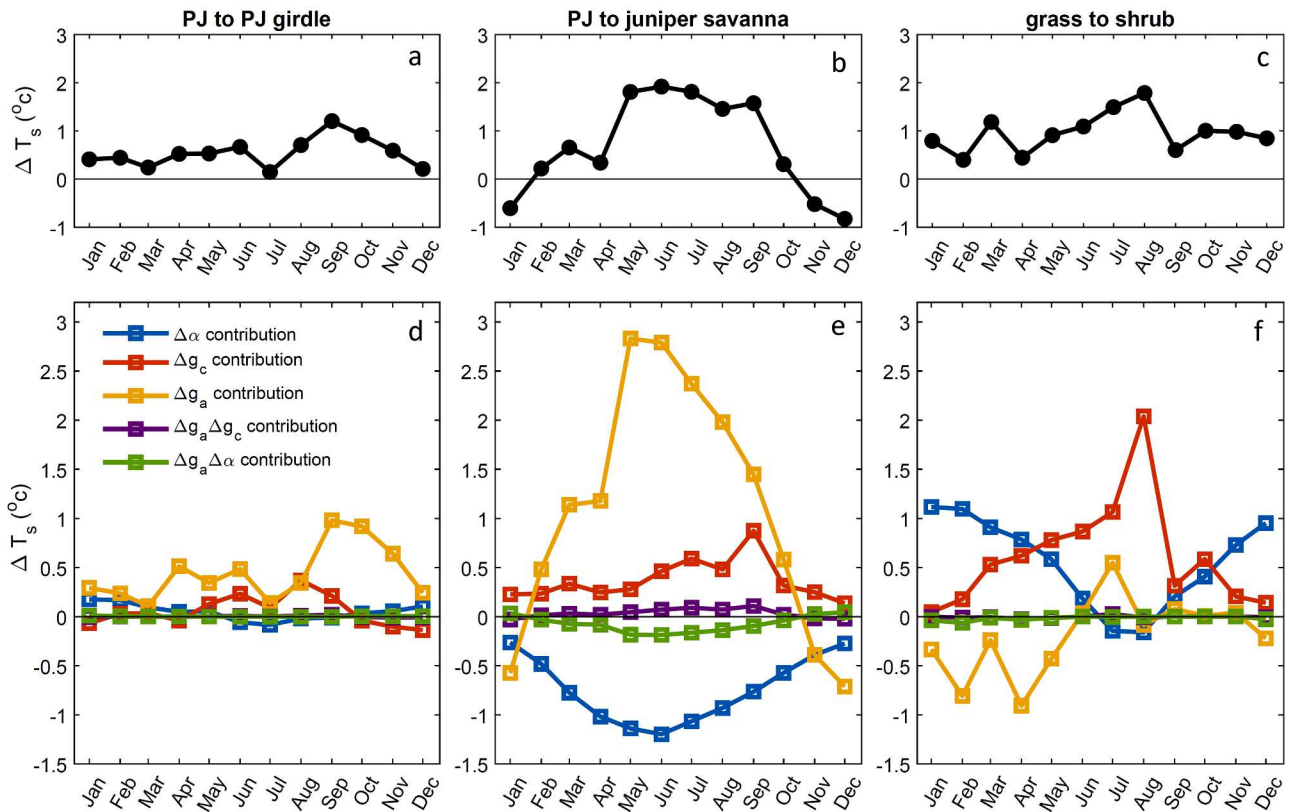
Fig. 3. (a,b,c) Monthly averaged changes in daytime surface temperature following changes in biophysical properties (albedo, aerodynamic conductance and canopy conductance). (d,e,f) The contribution of each of the components in equation (6) to ΔT_s. The contribution of Δg_a term here includes also the contribution of higher order terms (the contribution of the $(\Delta g_a)^2$ to $(\Delta g_a)^5$ terms). The contribution of each of the individual Δg_a terms is shown in Supplementary Fig. S3.

0.147±0.006 for before and after this LCC respectively (Fig. 2b). Complete removal of piñon trees decreases g_a for the majority of the year, except for an increase during the coldest months (November to January) (Fig. 2e). This LCC should also decrease g_c throughout the year (Fig. 2h), leading to an overall decrease in evaporative cooling in the juniper savanna compared to PJ (see change in *LE* following the LCC in Fig. S2). Our approach predicts that these changes in the biophysical variables alone could lead to an increase of about 2 degrees Celsius in daytime surface temperature during the growing season, from May to September (Fig. 3b). The main contributor to this increase is Δg_a, followed by Δg_c. The increase in T_s due to reduction in turbulent efficiency for heat transfer (lower g_a) and reduced evaporative cooling (lower g_c), was high enough to compensate for the cooling effect of change in albedo. In the transition months (February to April and October), the temperature increase due to Δg_a and Δg_c was balanced by the contribution of $\Delta\alpha$, resulting in a much smaller $\Delta T_s < 0.7$. In the winter coldest months (November to January) T_s decreased by 0.5 to 0.8 degrees, primarily due to the contribution of Δg_a which is negative during these months (Fig. 3e).

4.2. Impact of shrub encroachment on T_s

Our results suggest that if shrubs were added to our grass site, albedo would decrease (opposite of what was observed for the PJ to juniper savanna LCC) (Fig. 2c) and g_c would decrease throughout the entire year, similar to the long-term impacts of piñon mortality. However, the change in g_a is one-order of magnitude lower, predicting a much smaller effect of conversion from grass to shrub on the turbulence near the ground (Fig. 2i). As a result, T_s is predicted to increase from 0.4 to 1.8 degrees during the entire year (Fig. 3c). The predicted increase in daytime surface temperature is attributed to both albedo and Δg_c, interchangeably (Fig. 3f). Our simulation suggests that during the winter,

albedo is responsible for the increase, while Δg_c is the main contributor during the growing season. In this case, the only cooling agent following this LCC is Δg_a, and only during the winter months. However, the cooling impact of Δg_a is too small to counteract the heating effect of the other biophysical properties.

4.3. Interaction and high-order terms

For the PJ to juniper savanna LCC scenario we found that the contribution of the interaction terms ($\Delta\alpha\Delta g_a$ and $\Delta g_c\Delta g_a$) to surface temperature, while smaller than the contribution of the first order terms ($\Delta\alpha$, Δg_a, and Δg_c), is not negligible (Fig. 3e). Moreover, the second order contribution of Δg_a was in the same order of magnitude as the contribution of Δg_c (Fig. S3). These can be explained by the large perturbations in g_a in this study case.

For the PJ to PJ girdle and grass to shrub LCC scenarios, both the interaction terms (Fig. 3e,f) and the high-order terms (Fig. S3) had a negligible contribution to ΔT_s, due to the smaller perturbations in g_a. For these cases, ΔT_s calculated from L_{out} can be reconstructed using only the sum of the three first order terms in Eq. (6), while for PJ to juniper savanna LCC additional high order terms are required (Fig. S4).

4.4. Explaining the difference between observed and predicted ΔT_s using sensitivity analysis

The predicted change in daytime surface temperature due to changes in α, g_a and g_c is different from the observed daytime ΔT_s at the original study sites (Fig. 4). Given this discrepancy, we also used our approach to investigate to what degree this discrepancy can be explained by differences in non-biophysical properties between the original study-site pairs, such as soil water content, ground heat flux and air temperature. For each LCC conversion we explored how sensitive daytime
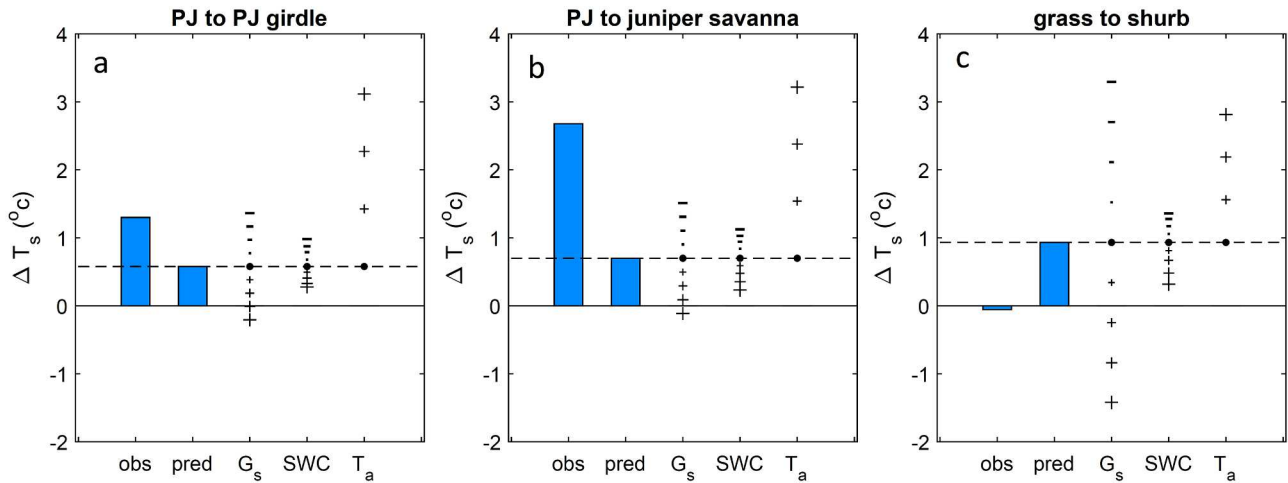
Fig. 4. The sensitivity of ΔT_s to changes in non-biophysical properties (G_s, *SWC*, and T_a) in addition to changes in biophysical properties (albedo, aerodynamic conductance and canopy conductance). In each panel, from left to right: obs is a yearly change in daytime temperatures as observed (from longwave outgoing radiation) between the two original measured datasets; pred stands for ΔT_s due to changes in albedo, aerodynamic conductance and canopy conductance only; the G_s and SWC show the effect of an additional increase or decrease of 5, 10, 15 and 20 percent in those properties, marked with a plus and minus signs respectively; the T_a bar shows the effect of increasing air temperature in 1,2 and 3°C in Site$_{post}$ compared to Site$_{pre}$.

surface temperature is to potential changes in *SWC*, G_s and T_a following LCC conversion, in addition to changes in α, g_a and g_c.

Daytime surface temperatures following all LCC scenarios were similarly sensitive to changes in *SWC*. An increase in *SWC* following both piñon mortality and creosote encroachment in our simulation, increased transpiration (through g_c) and therefore reduced daytime ΔT_s. A 20% increase in *SWC* could decrease T_s by approximately 0.5°C, and a 20% decrease in *SWC* could increase T_s by approximately 0.5°C (Fig. 4). A potential increase in ground heat flux following LCC would have a cooling effect. The grass to shrub LCC was much more sensitive to changes in G_s. An increase of 10% in G_s could reduce ΔT_s by ≈ 0.4°C following piñon mortality, but more than 1°C for shrub encroachment, thus potentially reversing the impact of the grass to shrub LCC on surface temperature from heating to cooling (Fig. 4). However, a change in G_s following grass to shrub LCC is less likely to be large, given that the difference in G_s at the original study sites (US-Seg and US-Ses) is less than 3% for the majority of the time (Fig. S5). An increase in T_a after conversion should lead to a direct increase in T_s in a ratio of 0.85:1, meaning 1 degree increase in T_a should lead to ≈ 0.85 degree increase in T_s.

Using the above sensitivity analysis for changes in non-biophysical properties, we can explain the differences between the observed and predicted ΔT_s. The observed difference between the US-Mpj and US-Wjs sites is 2°C higher than the predicted impact of piñon removal. We attribute this difference to a 3°C higher T_a in US-Wjs compared to US-Mpj (Fig. S5). In contrast, the observed difference between US-Mpj and US-Mpg is much more similar to the predicted short-term increase in temperature as a result of piñon mortality, since T_a in both sites is similar (Fig.S5). The slightly higher ΔT_s (0.7°C) in US-Mpg could be explained by lower SWC. For shrub encroachment, the observed difference in daytime surface temperature between US-Seg and US-Ses was close to zero, while the predicted ΔT_s was ≈ 1°C. This difference is unrelated to T_a which is relatively similar in both these study sites. It can be explained by a combination of differences in G_s and especially *SWC*, which is about 20% higher in US-Ses (Fig.S5). We additionally tested the sensitivity of ΔT_s to a scenario where T_a is increased for both before and after LCC, simulating the impact of LCC under conditions of elevated air temperature. For all LCC scenarios, elevated T_a had a negligible impact on ΔT_s, with a change of less than 0.1°C.

5. Discussion

5.1. Ts increases due to biophysical changes following both shrub encroachment and piñon mortality

Our approach predicted that the changes in biophysical properties in the LLC scenarios we examined should be sufficient to increase daytime T_s. The predicted increase averages around $\Delta T_s = 1$°C for all cases. In the short-term, considering only changes in biophysical properties and conserving all other environmental factors, our results indicate that piñon mortality (with dead snags standing) could lead to a mild increase in daytime surface temperature, agreeing with our hypothesis. For the decade following piñon mortality, the predicted average daytime surface temperature increase was 0.55°C compared to an undisturbed site, with similar heating around that value throughout the entire year. The potential long-term scenario of complete transition to juniper savanna, had a larger impact on T_s. Even though not all vegetation was removed in this scenario (as in deforestation), removing all piñon trees created a sparser canopy with higher surface temperature, that could reach to a maximum of about 2 degrees during the summer months. This increase is comparable to the increase in surface temperature that was found in studies that examined the impact of deforestation on surface temperature in temperate and tropical biomes. For example, comparing a hardwood forest and a pine plantation to a nearby open field, Juang et al. (2007) observed a difference in daytime surface temperatures averaged at 0.9 and 1.2 degrees respectively. Chen and Dirmeyer (2016) measured an increase of 2 degrees during daytime in AmeriFlux paired sites due to deforestation, and in Liao et al. (2018) daytime surface temperatures increased in 2-4 degrees in summer and 1-4 degrees in winter following deforestation. Additionally, Lee et al. (2011) observed an increase of 2 degrees in 24-hr averaged surface temperature due to deforestation in the tropics, and in Wang et al. (2018a) open land T_s was about 1 degree hotter than a sparse plantation in Mongolia desert during daytime in winter and spring.

Our approach predicted that shrub encroachment should increase T_s by 0.96±0.4°C throughout the entire year, contradicting our hypothesis. Although the observed difference between grass and shrub sites (US-Seg and US-Ses) in daytime surface temperature fits our hypothesis, with close to zero ΔT_s, this is explained by differences in soil water content at the study sites (US-Seg and US-Ses) rather than structural changes.

5.2. The role of LCC-driven perturbations in biophysical properties on increasing T_s

The impact of changes in the biophysical properties on surface temperature is summarized in the schematic diagram represented in Fig. 5. Even though all LCC scenarios we investigated increased surface temperature, the biophysical properties that contributed to these increases were unique to each LCC scenario. The contrasting contribution of albedo following shrub encroachment vs piñon mortality is especially interesting. The increase in albedo associated with PJ to juniper savanna conversion cooled the surface, similar to what has been observed in deforestation studies (Juang et al., 2007; Chen and Dirmeyer, 2016; Liao et al., 2018). However, the decrease in albedo heated the surface in the grassland to shrubland conversion, similar to what has been observed in boreal forest restoration studies (Bonan 2008; Jackson et al. 2008). The increase in temperature despite the increase in albedo, highlights the importance of including non-radiative processes to model the impact of land cover change on climate (Davin et al., 2007; Bonan 2008; Jackson et al. 2008).

The change in aerodynamic conductance was the largest contributor to heating when PJ is converted to juniper savanna. This heating was much larger than the predicted cooling effect of albedo. It was previously shown that replacing a forest with grass can decrease the aerodynamic conductance, such that it is the main contributor to surface heating in deforestation studies (Juang et al., 2007; Chen and Dirmeyer, 2016; Rigden and Li, 2017; Liao et al., 2018). Here, reducing the tree cover density has a similar effect, increasing surface temperature up to 3 degrees. Following shrub encroachment, the predicted changes in aerodynamic resistance should cool the system. However, heating due to reduced albedo following creosote encroachment surpassed the cooling due to increased aerodynamic conductance. Reduced evapotranspiration also contributed to heating, contradicting previous observations in Arizona associated with shrub encroachment (Scott et al., 2006). This suggests that the ecohydrological implications of woody plant encroachment can vary significantly depending on aridity level, water use efficiency of dominant species, percentage of vegetation cover vs bare ground, and potential access to groundwater (Huxman et al., 2005). In our study case, the change in canopy conductance following shrub encroachment without changes in environmental conditions, led to a decrease in latent heat flux which heated the surface, especially during the growing season.

5.3. Future implications of LCC in the Southwest US and uncertainties

We found that changes in biophysical characteristics associated with shrub encroachment and coniferous mortality events that are occurring over large areas in the Southwestern US could potentially lead to a warming of the surface comparable to the observed impacts following deforestation in many different biomes (Bonan, 2008; Jackson et al., 2008). However, the impact of LCCs on the hydrological system is harder to predict, leaving the future of water availability and changes in external atmospheric factors uncertain. According to our sensitivity analysis, if changes in climate and/or these LCCs also reduce water availability, surface temperatures could increase even more. Additionally, we found that surface temperature following both LCC's is sensitive to changes in ground heat flux, particularly following shrub encroachment. Our direct observations suggest that future increases in ground heat flux following piñon mortality will reduce the predicted surface warming. However, given the potential link between soil moisture and ground heat flux (Liebethal et al., 2005; Wang and Bou-Zeid, 2012), this decrease in surface temperature could be compensated by an increase due to drier soil conditions. Although surface temperature following shrub encroachment is very sensitive to changes in ground heat flux, our direct measurements suggest that shrub encroachment does not significantly alter midday ground heat flux. Overall, a continued increase in both shrub encroachment and piñon mortality could increase daytime temperatures in the Southwest US by at least 1 degree, due to biophysical changes alone.

We focused here only on the changes in biophysical components that impact radiative changes and evapotranspiration. Such changes can immediately impact the surface temperature locally at the short timescale. However, LCC can also modify carbon sequestration, which can potentially impact air temperature at larger spatial and temporal scales (Naudts et al., 2016; Luyssaert et al., 2018). Previous observations showed that the carbon sequestration strength at shrubland (US-Ses) is larger than at grassland (US_Seg), and larger in PJ (US-Mpj) compared to juniper savanna (US-Wjs) and the girdled site (US-Mpg) (Anderson-Teixeira et al., 2011; Petrie et al., 2015; Krofcheck et al., 2016). These differences in carbon sequestration could lead to cooling of the atmosphere following shrub encroachment, but warming following piñon mortality. However, future studies are required to understand how the increase or decrease in atmospheric CO_2 concentrations will interact with the radiative and non-radiative changes following LCC to
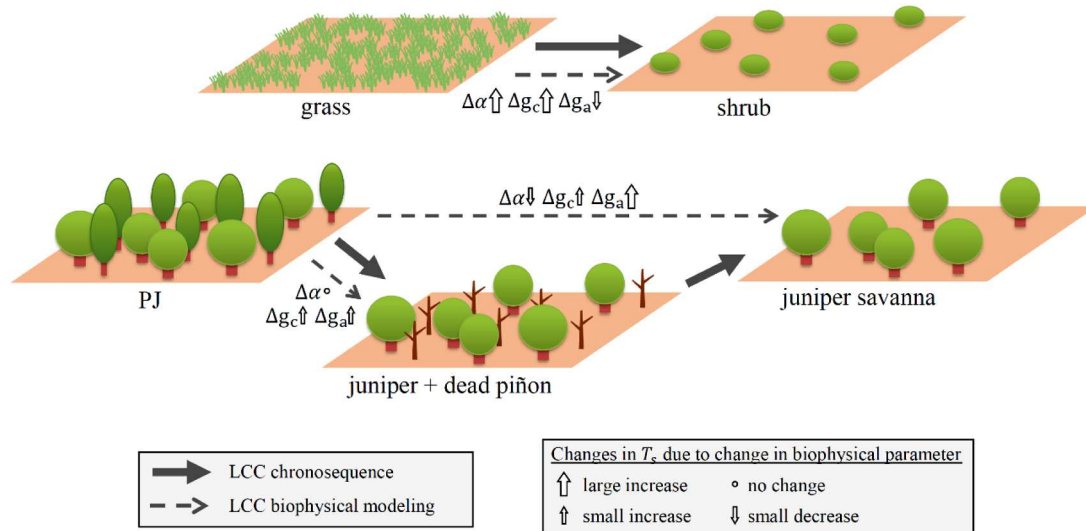

Fig. 5. Schematic representation of the LCCs scenarios studied in this work. The chronosequence is marked with solid arrows, while the LCC biophysical modeling is marked with dashed arrows directing from Site$_{pre}$ to Site$_{post}$. Also shown are the predicted impacts of changes in biophysical properties on daytime surface temperature.

impact air temperature. Our sensitivity analysis showed that elevated air temperature post-LCC compared to pre-LCC translated directly to an increase in surface temperature. However, the change in surface temperature was not impacted if air temperature is elevated both before and after the vegetation shift.

5.4. Modeling approach limitations and potential future improvements

We treated ground heat flux (G_s) as an environmental driver, in the same category as air temperature and incoming radiation. However, G_s can also vary with LCC. For simplicity, we explored the sensitivity of changes in surface temperature to changes in G_s by imposing incremental changes in the post-LCC site compared to the pre- LCC site (Sect. 3.2). Different approaches can be used to parameterize G_s as a function of other variables. It was previously suggested to link G_s with net radiation, total incoming radiation, or as a fraction of $H+LE$ (Purdy et al., 2016). G_s can be also linked to surface temperature and SWC (Wang and Bras, 1999; Wang and Bou-Zeid, 2012; Hsieh et al., 2009). However, this approach requires direct coupling with water balance and largely increases the model complexity. Future studies exploring such addition of different parameterizations for G_s to our modeling approach could provide additional information associated with the change in surface temperature following LCC.

Our decision to simplify the formulation of LE reduces the complexity of the Taylor expansion to estimate to contribution of changes in biophysical properties to changes in surface temperature. While this approach is appropriate during midday, where most of the time differences between g_c calculated from $LE=g_cL_vD/p_a$ and $LE=g_a g_c/(g_a+g_c) L_vD/p_a$ are minor, this is not the case when exploring changes in T_s during other times of the day, especially at nighttime. Additionally, the inclusion of stability corrections could increase the accuracy of this approach, especially during stable conditions during the night.

Finally, differences between aerodynamic surface temperature and radiometric surface temperature have been discussed previously in the literature (Stewart et al., 1994; Chehbouni et al., 1996). Differentiating between the surface temperature that is calculated from L_{out}, and the surface temperature that is used to model H (Eq. 2) requires additional modeling, and could be improved upon in future studies.

6. Conclusions

We show that shrub encroachment and conifer mortality that are both occurring in the Southwestern US can potentially lead to an increase in daytime surface temperature that is comparable to the effects of deforestation. The difference in measured daytime surface temperature at two sites can also reflect differences that are not directly related to the land cover, such as air temperature, soil heat flux and soil moisture. The novelty of our new methodology is that it can be used to predict how surface temperature will change due to perturbations in biophysical properties only, relying on functional responses of the system to environmental factors. The primary conclusion of our analysis is that extensive shrub encroachment and piñon mortality in the Southwest US could potentially lead to an increase of 1 to 2 degrees Celsius in daytime surface temperature. This increase in daytime surface temperature could be intensified with reduced soil water availability or increased air temperature following these land cover changes.

Declaration of Competing Interest

The authors declare that they have no known competing financial interests or personal relationships that could have appeared to influence the work reported in this paper.

Acknowledgements

Supplementary materials

Supplementary material associated with this article can be found, in the online version, at doi:10.1016/j.agrformet.2020.108246.

References

Anderegg, W.R., Hicke, J.A., Fisher, R.A., Allen, C.D., Aukema, J., Bentz, B., Hood, S., Lichstein, J.W., Macalady, A.K., McDowell, N., et al., 2015. . Tree mortality from drought, insects, and their interactions in a changing climate. New Phytol 208, 674–683.

Anderson-Teixeira, K.J., Delong, J.P., Fox, A.M., Brese, D.A., Litvak, M.E., 2011. Differential responses of production and respiration to temperature and moisture drive the carbon balance across a climatic gradient in New Mexico. Global Change Biol 17 (1), 410–424.

Báez, S., Collins, S.L., 2008. Shrub invasion decreases diversity and alters community stability in northern chihuahuan desert plant communities. PLoS One 3.

Baldocchi, D., Ma, S., 2013. How will land use affect air temperature in the surface boundary layer? Lessons learned from a comparative study on the energy balance of an oak savanna and annual grassland in California. USA. Tellus B: Chem. Phys. Meteorol. 65, 19994. https://doi.org/10.3402/tellusb.v65i0.19994.

Bathiany, S., Claussen, M., Brovkin, V., Raddatz, T., Gayler, V., 2010. Combined biogeophysical and biogeochemical effects of large-scale forest cover changes in the MPI earth system model. Biogeosciences 7, 1383–1399. https://doi.org/10.5194/bg-7-1383-2010.

Biederman, J.A., Scott, R.L., Bell, T.W., Bowling, D.R., Dore, S., GaratuzaPayan, J., Kolb, T.E., Krishnan, P., Krofcheck, D.J., Litvak, M.E., Maurer, G.E., Meyers, T.P., Oechel, W.C., Papuga, S.A., Ponce-Campos, G.E., Rodriguez, J.C., Smith, W.K., Vargas, R., Watts, C.J., Yepez, E.A., Goulden, M.L., 2017. CO2 exchange and evapotranspiration across dryland ecosystems of southwestern North America. Global Change Biol 23, 4204–4221. https://doi.org/10.1111/gcb.13686.

Bonan, G.B., 2008. Forests and Climate Change: Forcings, Feedbacks, and the Climate Benefits of Forests. Science 320, 1444–1449. https://doi.org/10.1126/science.1155121.

Breshears, D.D., Myers, O.B., Meyer, C.W., Barnes, F.J., Zou, C.B., Allen, C.D., McDowell, N.G., Pockman, W.T., 2009. Tree die-off in response to global change-type drought: Mortality insights from a decade of plant water potential measurements. Front. Earth Sci. 7, 185–189. https://doi.org/10.1890/080016.

Brewer, W.L., Lippitt, C.L., Lippitt, C.D., Litvak, M.E., 2017. Assessing drought-induced change in a piñon-juniper woodland with Landsat: A multiple endmember spectral mixture analysis approach. Int. J. Remote Sens. 38, 4156–4176. https://doi.org/10.1080/01431161.2017.1317940.

Buffington, L.C., Herbel, C.H., 1965. Vegetational Changes on a Semidesert Grassland Range from 1858 to 1963. Ecol. Monogr. 35, 139–164, 10. 2307/1948415.

Burakowski, E., Tawfik, A., Ouimette, A., Lepine, L., Novick, K., Ollinger, S., Zarzycki, C., Bonan, G., 2018. The role of surface roughness, albedo, and Bowen ratio on ecosystem energy balance in the Eastern United States. Agric. For. Meteorol. 249, 367–376. https://doi.org/10.1016/j.agrformet.2017.11.030.

Caracciolo, D., Istanbulluoglu, E., Noto, L.V., Collins, S.L., 2016. Mechanisms of shrub encroachment into Northern Chihuahuan Desert grasslands and impacts of climate change investigated using a cellular automata model. Adv. Water Resour. 91, 46–62.

Cayan, D.R., Das, T., Pierce, D.W., Barnett, T.P., Tyree, M., Gershunov, A., 2010. Future dryness in the southwest US and the hydrology of the early 21st century drought. Proc. Natl. Acad. Sci. 107 (50), 21271–21276.

Chen, L., Dirmeyer, P.A., 2016. Adapting observationally based metrics of biogeophysical feedbacks from land cover/land use change to climate modeling. Environ. Res. Lett. 11, 034002 https://doi.org/10.1088/1748-9326/11/3/034002.

Chehbouni, A., Seen, D.L., Njoku, E.G., Monteny, B.M., 1996. Examination of the difference between radiative and aerodynamic surface temperatures over sparsely vegetated surfaces. Remote Sens. Environ. 58 (2), 177–186.

Clifford, M.J., Cobb, N.S., Buenemann, M., 2011. Long-Term Tree Cover Dynamics in a Pinyon-Juniper Woodland: Climate-Change-Type Drought Resets Successional Clock. Ecosystems 14, 949–962, 10.1007/ s10021-011-9458-2.

Cook, B.I., Ault, T.R., Smerdon, J.E., 2015. Unprecedented 21st century drought risk in the American Southwest and Central Plains. Sci. Adv. 1 (1), e1400082.

Davin, E.L., de Noblet-Ducoudré, N., 2010. Climatic Impact of Global-Scale Deforestation: Radiative versus Nonradiative Processes. J. Clim. 23, 97–112. https://doi.org/10.1175/2009JCLI3102.1.

Davin, E.L., de Noblet-Ducoudré, N., Friedlingstein, P., 2007. Impact of land cover change on surface climate: Relevance of the radiative forcing concept. Geophys. Res. Lett. 34 https://doi.org/10.1029/2007GL029678.

Devaraju, N., Bala, G., Nemani, R., 2015. Modelling the influence of land-use changes on biophysical and biochemical interactions at regional and global scales. Plant Cell Environ 38, 1931–1946. https://doi.org/10.1111/pce.12488.

Devaraju, N., de Noblet-Ducoudré, N., Quesada, B., Bala, G., 2018. Quantifying the Relative Importance of Direct and Indirect Biophysical Effects of Deforestation on Surface Temperature and Teleconnections. J. Clim. 31, 3811–3829. https://doi.org/10.1175/JCLI-D-17-0563.1.

D'Odorico, P., Fuentes, J.D., Pockman, W.T., Collins, S.L., He, Y., Medeiros, J.S., DeWekker, S., Litvak, M.E., 2010. Positive feedback between microclimate and shrub encroachment in the northern Chihuahuan desert. Ecosphere 1. https://doi.org/10.1890/ES10-00073.1 art17.

He, Y., D'Odorico, P., De Wekker, S.F., 2015. The role of vegetation– microclimate feedback in promoting shrub encroachment in the northern chihuahuan desert. Global Change Biol 21, 2141–2154.

He, Y., D'Odorico, P., De Wekker, S.F.J., Fuentes, J.D., Litvak, M., 2010. On the impact of shrub encroachment on microclimate conditions in the northern Chihuahuan desert. J. Geophys. Res. Atmos. 115, 10.1029/ 2009JD013529.

Hsieh, C.I., Huang, C.W., Kiely, G., 2009. Long-term estimation of soil heat flux by single layer soil temperature. Int. J. Biometeorol. 53 (1), 113–123.

Huang, C.W., Krofcheck, D., Duman, T., Fox, A., Pockman, W., Lippit, C., McIntire, C., Litvak, M., 2020. Ecosystem-level energy and water budgets are resilient to canopy mortality in sparse semi-arid biomes. J. Geophys. Res. Biogeosci. https://doi.org/10.1029/2020JG005858.

Huxman, T.E., Wilcox, B.P., Breshears, D.D., Scott, R.L., Snyder, K.A., Small, E.E., Hultine, K., Pockman, W.T., Jackson, R.B., 2005. Ecohydrological implications of woody plant encroachment. Ecology 86, 308–319, 10. 1890/03-0583.

Jackson, R.B., Randerson, J.T., Canadell, J.G., Anderson, R.G., Avissar, R., Baldocchi, D. D., Bonan, G.B., Caldeira, K., Diffenbaugh, N.S., Field, C.B., Hungate, B.A., 2008. Protecting climate with forests. Environ. Res. Lett. 3 (4), 044006.

Juang, J.Y., Katul, G., Siqueira, M., Stoy, P., Novick, K., 2007. Separating the effects of albedo from eco-physiological changes on surface temperature along a successional chronosequence in the southeastern United States. Geophys. Res. Lett. 34 https://doi.org/10.1029/2007GL031296.

Krofcheck, D.J., Eitel, J.U., Lippitt, C.D., Vierling, L.A., Schulthess, U., Litvak, M.E., 2016. Remote sensing based simple models of GPP in both disturbed and undisturbed Piñon-Juniper woodlands in the Southwestern US. Remote sens 8, 20.

Krofcheck, D.J., Eitel, J.U., Vierling, L.A., Schulthess, U., Hilton, T.M., Dettweiler-Robinson, E., Pendleton, R., Litvak, M.E., 2014. Detecting mortality induced structural and functional changes in a piñon -juniper woodland using landsat and rapideye time series. Remote Sens. Environ. 151, 102–113.

Lee, X., Goulden, M.L., Hollinger, D.Y., Barr, A., Black, T.A., Bohrer, G., Bracho, R., Drake, B., Goldstein, A., Gu, L., Katul, G., Kolb, T., Law, B.E., Margolis, H., Meyers, T., Monson, R., Munger, W., Oren, R., Paw U, K.T., Richardson, A.D., Schmid, H.P., Staebler, R., Wofsy, S., Zhao, L., 2011. Observed increase in local cooling effect of deforestation at higher latitudes. Nature 479, 384–387. https://doi.org/10.1038/nature10588.

Levis, S., 2010. Modeling vegetation and land use in models of the Earth System. Wiley Interdisciplinary Reviews: Climate Change 1, 840–856, 10.1002/ wcc.83.

Li, Z., Deng, X., Shi, Q., Ke, X., Liu, Y., 2013. Modeling the Impacts of Boreal Deforestation on the Near-Surface Temperature in European Russia. Adv. Meteorol. https://doi.org/10.1155/2013/486962.

Liao, W., Rigden, A.J., Li, D., 2018. Attribution of Local Temperature Response to Deforestation. J. Geophys. Res. Biogeosci. 123, 1572–1587, 10.1029/ 2018JG004401.

Liebethal, C., Huwe, B., Foken, T., 2005. Sensitivity analysis for two ground heat flux calculation approaches. Agric. For. Meteorol. 132, 253–262.

Luyssaert, S., Jammet, M., Stoy, P.C., Estel, S., Pongratz, J., Ceschia, E., Churkina, G., Don, A., Erb, K., Ferlicoq, M., Gielen, B., Grünwald, T., Houghton, R.A., Klumpp, K., Knohl, A., Kolb, T., Kuemmerle, T., Laurila, T., Lohila, A., Loustau, D., McGrath, M. J., Meyfroidt, P., Moors, E.J., Naudts, K., Novick, K., Otto, J., Pilegaard, K., Pio, C.A., Rambal, S., Rebmann, C., Ryder, J., Suyker, A.E., Varlagin, A., Wattenbach, M., Dolman, A.J., 2014. Land management and land-cover change have impacts of similar magnitude on surface temperature. Nat. Clim. Change 4, 389–393. https://doi.org/10.1038/nclimate2196.

Luyssaert, S., Marie, G., Valade, A., Chen, Y.Y., Djomo, S.N., Ryder, J., Otto, J., Naudts, K., Lansø, A.S., Ghattas, J., McGrath, M.J., 2018. Trade-offs in using European forests to meet climate objectives. Nature 562 (7726), 259–262.

Mahmood, R., Pielke, R.A., Hubbard, K.G., Niyogi, D., Dirmeyer, P.A., McAlpine, C., Carleton, A.M., Hale, R., Gameda, S., Beltrán-Przekurat, A., Baker, B., McNider, R., Legates, D.R., Shepherd, M., Du, J., Blanken, P.D., Frauenfeld, O.W., Nair, U., Fall, S., 2014. Land cover changes and their biogeophysical effects on climate. Int. J. Clim. 34, 929–953. https://doi.org/10.1002/joc.3736.

Matthews, H.D., Weaver, A.J., Meissner, K.J., Gillett, N.P., Eby, M., 2004. Natural and anthropogenic climate change: Incorporating historical land cover change, vegetation dynamics and the global carbon cycle. Clim. Dyn. 22, 461–479. https://doi.org/10.1007/s00382-004-0392-2.

Morillas, L., Pangle, R.E., Maurer, G.E., Pockman, W.T., McDowell, N., Huang, C.W., Krofcheck, D.J., Fox, A.M., Sinsabaugh, R.L., Rahn, T.A., Litvak, M.E., 2017. Tree Mortality Decreases Water Availability and Ecosystem Resilience to Drought in Piñon -Juniper Woodlands in the Southwestern U.S. J. Geophys. Res. Biogeosci. 122, 3343–3361. https://doi.org/10.1002/2017JG004095.

Naudts, K., Chen, Y., McGrath, M.J., Ryder, J., Valade, A., Otto, J., Luyssaert, S., 2016. Europe's forest management did not mitigate climate warming. Science 351 (6273), 597–600.

Petrie, M.D., Collins, S.L., Swann, A.M., Ford, P.L., Litvak, M.E., 2015. Grassland to shrubland state transitions enhance carbon sequestration in the northern Chihuahuan Desert. Global Change Biol 21, 1226–1235. https://doi.org/10.1111/gcb.12743.

Pielke, R.A., Pitman, A., Niyogi, D., Mahmood, R., McAlpine, C., Hossain, F., Goldewijk, K.K., Nair, U., Betts, R., Fall, S., Reichstein, M., Kabat, P., de Noblet, N., 2011. Land use/land cover changes and climate: Modeling analysis and observational evidence. Wiley Interdisciplinary Reviews: Climate Change 2, 828–850. https://doi.org/10.1002/wcc.144.

Purdy, A.J., Fisher, J.B., Goulden, M.L., Famiglietti, J.S., 2016. Ground heat flux: An analytical review of 6 models evaluated at 88 sites and globally. J. Geophys. Res. Biogeosci. 121 (12), 3045–3059.

Raffa, K.F., Aukema, B.H., Bentz, B.J., Carroll, A.L., Hicke, J.A., Turner, M.G., Romme, W.H., 2008. Cross-scale drivers of natural disturbances prone to anthropogenic amplification: the dynamics of bark beetle eruptions. Bioscience 58, 501–517.

Rigden, A.J., Li, D., 2017. Attribution of surface temperature anomalies induced by land use and land cover changes. Geophys. Res. Lett. 44, 6814–6822. https://doi.org/10.1002/2017GL073811.

Romme, W.H., Allen, C.D., Bailey, J.D., Baker, W.L., Bestelmeyer, B.T., Brown, P.M., Eisenhart, K.S., Floyd, M.L., Huffman, D.W., Jacobs, B.F., Miller, R.F., Muldavin, E. H., Swetnam, T.W., Tausch, R.J., Weisberg, P.J., 2009. Historical and Modern Disturbance Regimes, Stand Structures, and Landscape Dynamics in Piñon –Juniper Vegetation of the Western United States. Rangeland Ecol. Manage. 62, 203–222. https://doi.org/10.2111/08-188R1.1.

Scott, R.L., Huxman, T.E., Williams, D.G., Goodrich, D.C., 2006. Ecohydrological impacts of woody-plant encroachment: Seasonal patterns of water and carbon dioxide exchange within a semiarid riparian environment. Global Change Biol 12, 311–324.

Seager, R., Ting, M., Held, I., Kushnir, Y., Lu, J., Vecchi, G., Huang, H.P., Harnik, N., Leetmaa, A., Lau, N.C., Li, C., 2007. Model projections of an imminent transition to a more arid climate in southwestern North America. Science 316 (5828), 1181–1184.

Shaw, J.D., Steed, B.E., DeBlander, L.T., 2005. Forest Inventory and Analysis (FIA) Annual Inventory Answers the Question: What Is Happening to Pinyon-Juniper Woodlands? J. For 103, 280–285. https://doi.org/10.1093/jof/103.6.280.

Stewart, J.B., Kustas, W.P., Humes, K.S., Nichols, W.D., Moran, M.S., de Bruin, H.A., 1994. Sensible heat flux-radiometric surface temperature relationship for eight semiarid areas. J. Appl. Meteor. 33 (9), 1110–1117.

Swetnam, T.W., Betancourt, J.L., 1998. Mesoscale disturbance and ecological response to decadal climatic variability in the american southwest. J. Clim. 11, 3128–3147.

Van Auken, O.W., 2000. Shrub Invasions of North American Semiarid Grasslands. Annu. Rev. Ecol. Syst. 31, 197–215, 10.1146/annurev.ecolsys. 31.1.197.

Van Auken, O.W., 2009. Causes and consequences of woody plant encroachment into western North American grasslands. J. Environ. Manage. 90, 2931–2942. https://doi.org/10.1016/j.jenvman.2009.04.023.

Van Mantgem, P.J., Stephenson, N.L., Byrne, J.C., Daniels, L.D., Franklin, J.F., Fulé, P.Z., Harmon, M.E., Larson, A.J., Smith, J.M., Taylor, A.H., et al., 2009. Widespread increase of tree mortality rates in the western united states. Science 323, 521–524.

Vanden Broucke, S., Luyssaert, S., Davin, E.L., Janssens, I., van Lipzig, N., 2015. New insights in the capability of climate models to simulate the impact of LUC based on temperature decomposition of paired site observations. J. Geophys. Res. Atmos. 120, 5417–5436. https://doi.org/10.1002/2015JD023095.

Wang, J., Bras, R.L., 1999. Ground heat flux estimated from surface soil temperature. J. hydrol. 216 (3-4), 214–226.

Wang, L., Lee, X., Schultz, N., Chen, S., Wei, Z., Fu, C., Gao, Y., Yang, Y., Lin, G., 2018a. Response of Surface Temperature to Afforestation in the Kubuqi Desert, Inner Mongolia. J. Geophys. Res. Atmos 123, 948–964. https://doi.org/10.1002/2017JD027522.

Wang, P., Li, X.Y., Wang, L., Wu, X., Hu, X., Fan, Y., Tong, Y., 2018b. Divergent evapotranspiration partition dynamics between shrubs and grasses in a shrub-encroached steppe ecosystem. New Phytol 219, 1325–1337.

Wang, Z.H., Bou-Zeid, E., 2012. A novel approach for the estimation of soil ground heat flux. Agric. For. Meteorol. 154, 214–221.

Warnock, D.D., Litvak, M.E., Morillas, L., Sinsabaugh, R.L., 2016. Droughtinduced piñon mortality alters the seasonal dynamics of microbial activity in piñon –juniper woodland. Soil Biol. Biochem. 92, 91–101. https://doi.org/10.1016/j.soilbio.2015.09.007.

Webb, E.K., Pearman, G.I., Leuning, R., 1980. Correction of flux measurements for density effects due to heat and water vapour transfer. Quart. J. Roy. Meteorol. Soc. 106, 85–100. https://doi.org/10.1002/qj.49710644707.

Westerling, A.L., Hidalgo, H.G., Cayan, D.R., Swetnam, T.W., 2006. Warming and earlier spring increase western us forest wildfire activity. Science 313, 940–943.

Westerling, A.L., Swetnam, T.W., 2003. Interannual to decadal drought and wildfire in the western united states. EOS, Transactions American Geophysical Union 84, 545–555.

Williams, A.P., Allen, C.D., Macalady, A.K., Griffin, D., Woodhouse, C.A., Meko, D.M., Swetnam, T.W., Rauscher, S.A., Seager, R., Grissino-Mayer, H.D., et al., 2013. . Temperature as a potent driver of regional forest drought stress and tree mortality. Nat. Clim. Change 3, 292–297.

Williams, A.P., Allen, C.D., Millar, C.I., Swetnam, T.W., Michaelsen, J., Still, C.J., Leavitt, S.W., 2010. Forest responses to increasing aridity and warmth in the southwestern united states. Proc. Natl. Acad. Sci. 107, 21289–21294.

Winckler, J., Reick, C.H., Pongratz, J., 2016. Robust Identification of Local Biogeophysical Effects of Land-Cover Change in a Global Climate Model. J. Clim. 30, 1159–1176. https://doi.org/10.1175/JCLI-D-16-0067.1.

Zhang, M., Lee, X., Yu, G., Han, S., Wang, H., Yan, J., Zhang, Y., Li, Y., Ohta, T., Hirano, T., Kim, J., Yoshifuji, N., Wang, W., 2014. Response of surface air temperature to small-scale land clearing across latitudes. Environ. Res. Lett. 9, 034002 https://doi.org/10.1088/1748-9326/9/3/034002.

Zhao, K., Jackson, R.B., 2014. Biophysical forcings of land-use changes from potential forestry activities in North America. Ecol. Monogr. 84, 329–353. https://doi.org/10.1890/12-1705.1.